**ELECTRONIC SUPPLEMENTARY INFORMATION**

# A study across scales to unveil microstructural regimes in the multivalent metal driven self-assembly of cellulose nanocrystals

*Valeria Gabrielli*[a], *Alberta Ferrarini*[a,*] *and Marco Frasconi*[a,*]

[a] Department of Chemical Sciences, University of Padova, Via Marzolo 1, 35131 Padova, Italy

* E-mail: alberta.ferrarini@unipd.it; marco.frasconi@unipd.it

## Contents

## 1. NMR characterization of TOCNC-$Fe^{3+}$ sol structure and dynamics

*$^{1}H$-$^{13}C$ HSCQ NMR – signal decay upon $Fe^{3+}$ titration*

**Table S1.** Ratio of TOCNC 1wt% C peaks integrals in the absence and in the presence (1, 2, 3, 4, and 5 mM) of $Fe^{3+}$ acquired with a relaxation delay of 2 seconds.

| *$Fe^{3+}$ [mM]* | *C1c* | *C1r* | *C2c* | *C2r* | *C4nr* | *C3nr* | *C4r* | *C4c* | *C3,5c* | *C3,5ox* | *C5nr* | *C5r* | *C3r* | *C6c* |
|---|---|---|---|---|---|---|---|---|---|---|---|---|---|---|
| *0* | 1 | 1 | 1 | 1 | 1 | 1 | 1 | 1 | 1 | 1 | 1 | 1 | 1 | 1 |
| *1* | 0.81 | 0.87 | 0.80 | 0.78 | 0.73 | 0.73 | 0.72 | 0.82 | 0.80 | 0.84 | 0.78 | 0.89 | 0.79 | 0.72 |
| *2* | 0.69 | 0.74 | 0.67 | 0.52 | 0.62 | 0.58 | 0.50 | 0.64 | 0.68 | 0.54 | 0.55 | 0.67 | 0.63 | 0.60 |
| *3* | 0.54 | 0.53 | 0.56 | 0.44 | 0.37 | 0.36 | 0.38 | 0.57 | 0.45 | 0.32 | 0.42 | 0.34 | 0.45 | 0.41 |
| *4* | 0.38 | 0.29 | 0.39 | 0.2 | 0.14 | 0.12 | 0.25 | 0.47 | 0.30 | 0.05 | 0.14 | 0.20 | 0.31 | 0.27 |
| *5* | 0.29 | 0.21 | 0.27 | ns | ns | ns | ns | 0.23 | 0.18 | ns | ns | ns | ns | ns |
| LSD fit | -0.14 | -0.20 | -0.14 | -0.19 | -0.20 | -0.20 | -0.19 | -0.14 | -0.17 | -0.22 | -0.20 | -0.21 | -0.19 | -0.19 |
| $R^2$ | 0.99 | 0.98 | 0.99 | 0.99 | 0.99 | 0.99 | 0.98 | 0.98 | 0.99 | 0.98 | 0.99 | 0.99 | 0.98 | 0.99 |

**Table S2.** Ratio of TOCNC 1wt% C peaks integrals in the absence and in the presence (1, 2, 3, 4, and 5 mM) of $Fe^{3+}$ acquired with a relaxation delay of 60 seconds.

| *$Fe^{3+}$ [mM]* | *C1c* | *C1r* | *C2c* | *C2r* | *C4nr* | *C3nr* | *C4r* | *C4c* | *C3,5c* | *C3,5ox* | *C5nr* | *C5r* | *C3r* | *C6c* |
|---|---|---|---|---|---|---|---|---|---|---|---|---|---|---|
| *0* | 1 | 1 | 1 | 1 | 1 | 1 | 1 | 1 | 1 | 1 | 1 | 1 | 1 | 1 |
| *1* | 0.80 | 0.83 | 0.83 | 0.76 | 0.77 | 0.69 | 0.64 | 0.83 | 0.83 | 0.80 | 0.76 | 0.88 | 0.74 | 0.69 |
| *3* | 0.48 | 0.44 | 0.57 | 0.35 | 0.36 | 0.30 | 0.28 | 0.52 | 0.39 | 0.27 | 0.37 | 0.30 | 0.37 | 0.4 |
| *5* | 0.09 | 0.1 | 0.25 | ns | ns | ns | ns | 0.22 | 0.10 | ns | ns | ns | ns | ns |
| LSD fit | -0.18 | -0.18 | -0.15 | -0.20 | -0.20 | -0.20 | -0.19 | -0.16 | -0.18 | -0.21 | -0.20 | -0.21 | -0.20 | -0.19 |
| $R^2$ | 1 | 1 | 1 | 1 | 1 | 0.98 | 0.97 | 1 | 0.99 | 0.98 | 1 | 0.98 | 1 | 0.99 |

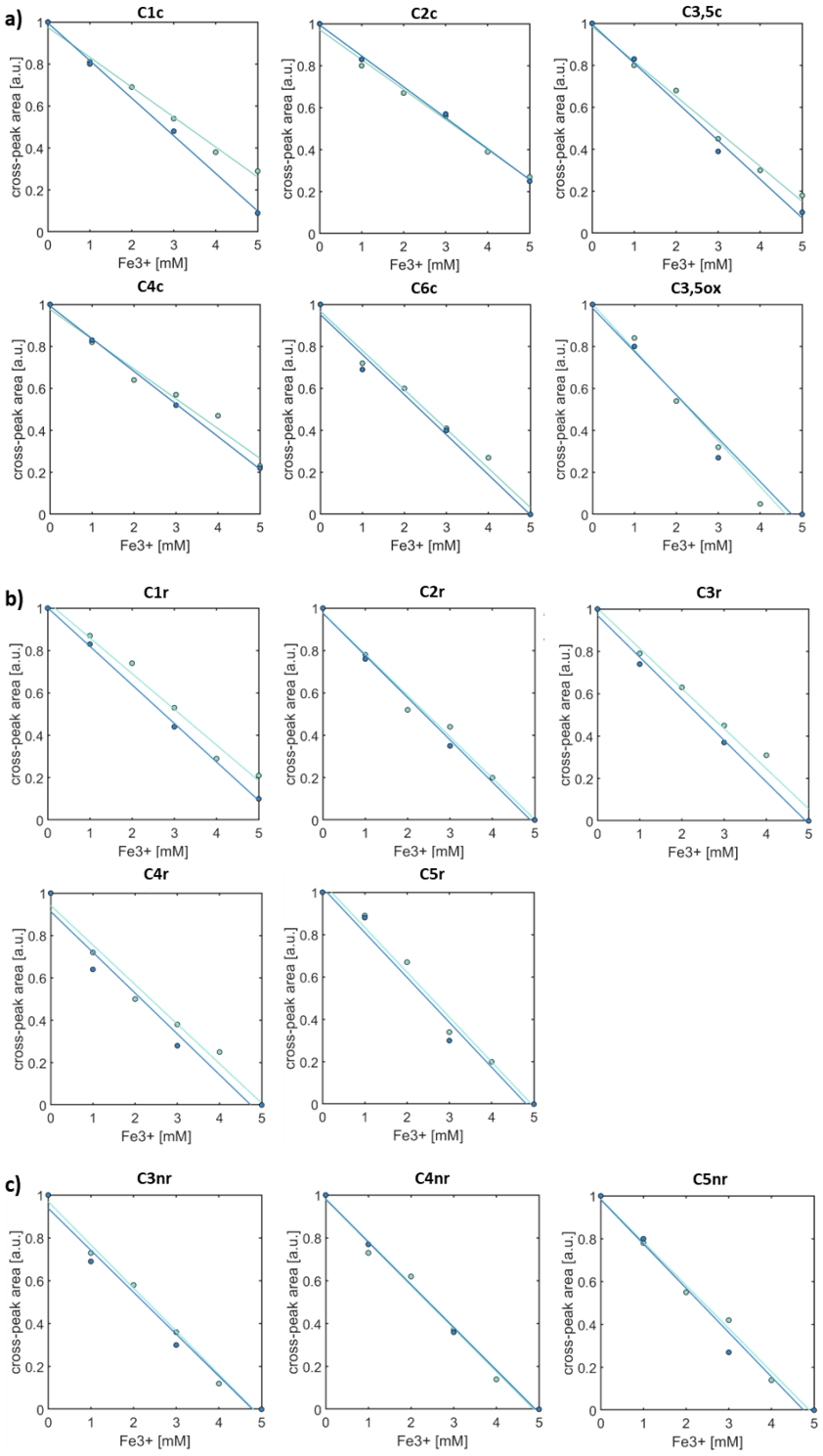


**Fig. S1.** Comparison of the decay of the cross-peaks' intensity for the 2D $^{1}H$-$^{13}C$ HSQC spectra of TOCNC 1wt% acquired at different relaxation delays (2 and 60 seconds in light blue and dark blue, respectively) upon titration with $Fe^{3+}$ ions, concentration ranging from 0 to 5 mM. The identified spin systems are divided as central carbons (a) and as carbons corresponding to the reducing- (b) and non-reducing end (c) sides.

*Conformational changes with $^{1}H$-$^{1}H$ NOESY experiments*

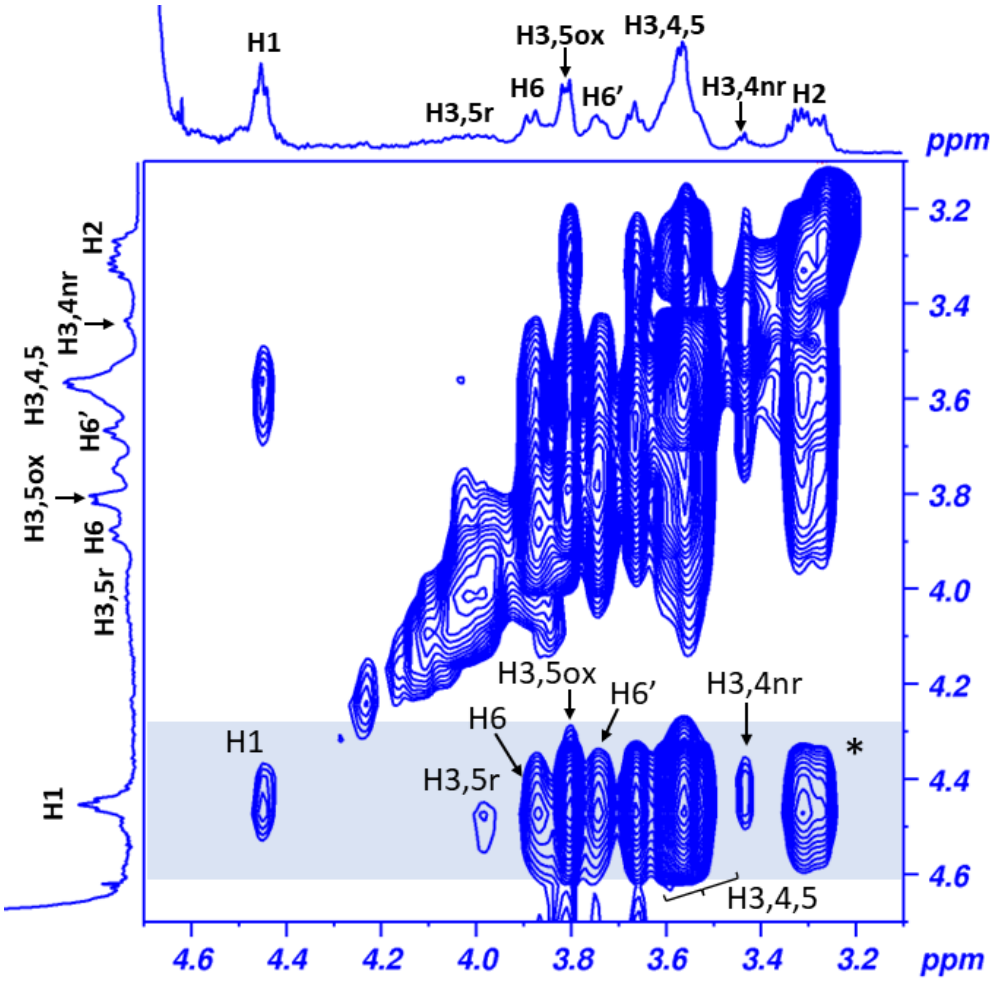


**Fig. S2** NOESY spectrum of a dispersion of TOCNC 1wt% at 25 °C and 600 ms mixing time.

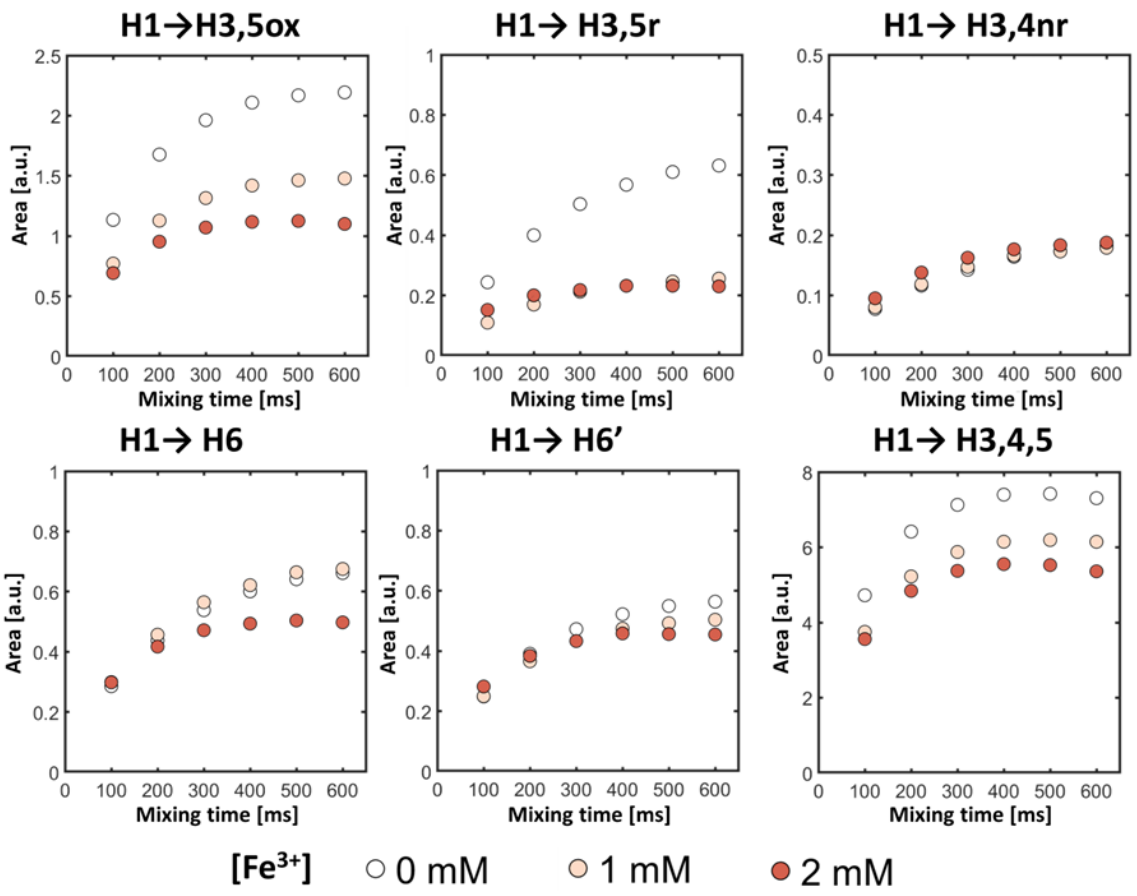


**Fig. S3.** Absolute NOE cross-peaks values of TOCNC 1wt% upon titration of $Fe^{3+}$. [$Fe^{3+}$]: 0 (white), 1 (yellow) and 2 (orange) mM.

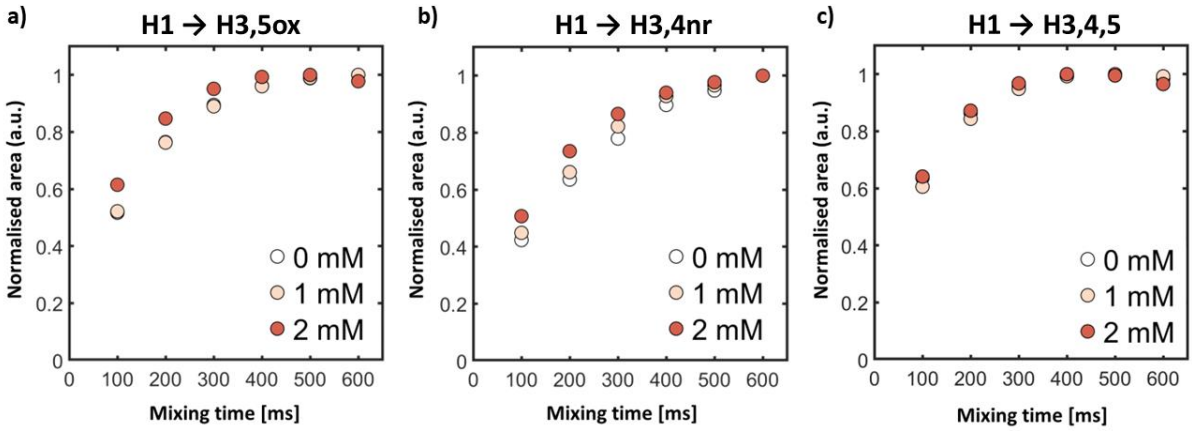


**Fig. S4.** Normalised NOE cross-peaks values of TOCNC 1wt% upon titration of $Fe^{3+}$.

*Water structuration changes upon $Fe^{3+}$ titration*

- *STD NMR experiments*

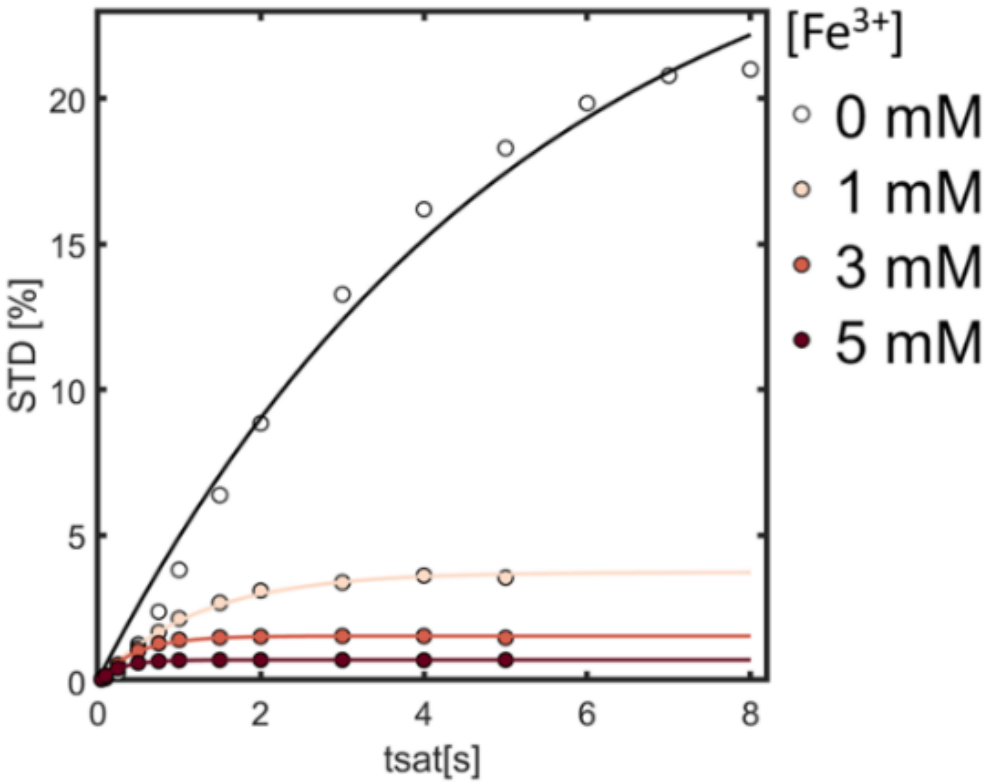


**Fig. S5.** STD build-up curves of TOCNC 1wt% upon titration of $Fe^{3+}$ ions.

- *SDTD NMR experiments*

The SDTD build-up curves were then fitted to the SDTD equation, derived from Fick's second law of diffusion:

$$SDTD = C \cdot erfc\left[\frac{r}{2 \cdot \sqrt{D_{SD} \cdot t_{sat}}} - b\right] \quad (4)$$

where *SDTD* is the normalised STD intensity values, *C* is the proportionality constant of the fit, *erfc* is the complementary error function, *r* is the minimum distance between the gelator particles and HDO molecules (expressed in nm), $D_{SD}$ is the spin diffusion coefficient at the particle-solvent interface (expressed in $nm^2/ms$), $t_{sat}$ is the saturation time (expressed in ms) and *b* is a correction factor to center the Gaussian distribution. Fitting of the curves was performed by keeping the *r* and *b* parameters constant. The r parameter was set to 2 Å, a value already reported for water-particle interfaces. For the *b* parameter, several values were tested until the best fit was obtained. Importantly, the dependence of $D_{SD}$ on the *b* value used during the fit determines that only $D_{SD}$ values obtained from curve fits processed with the same *b* value can be compared.

**Table S3.** Calculated values for the *C* and *D* parameters obtained from the fit to *Equation 4* of the SDTD build-up curves of the HDO peak for the TOCNC 1wt% dispersions without and with the presence of $Fe^{+3}$ ions. An *r* value of 0.2 nm and a *b* value of 2 were kept constant during the fit. For the *b* parameter, several values were tested to achieve the best fit. The errors associated to each *C* and *D* value are shown in parenthesis and correspond to the 99% confidence level. The $R^2$ values of each fit to *Equation 4* are shown.

| **$Fe^{3+}$ [mM]** | **0** | **1** | **3** | **5** |
|---|---|---|---|---|
| **C** | 0.59 (±0.04) | 0.53 (±0.03) | 0.52 (±0.03) | 0.51 (±0.02) |
| **D** | 0.00068 (± 4.72E-05) | 0.00122 (± 8.18E-05) | 0.00197 (± 2.04E-04) | 0.00260 (± 2.45E-04) |
| **$R^2$** | 0.995 | 0.996 | 0.992 | 0.992 |

## 2. Electrochemical characterization of the TOCNC-$Fe^{3+}$ complex

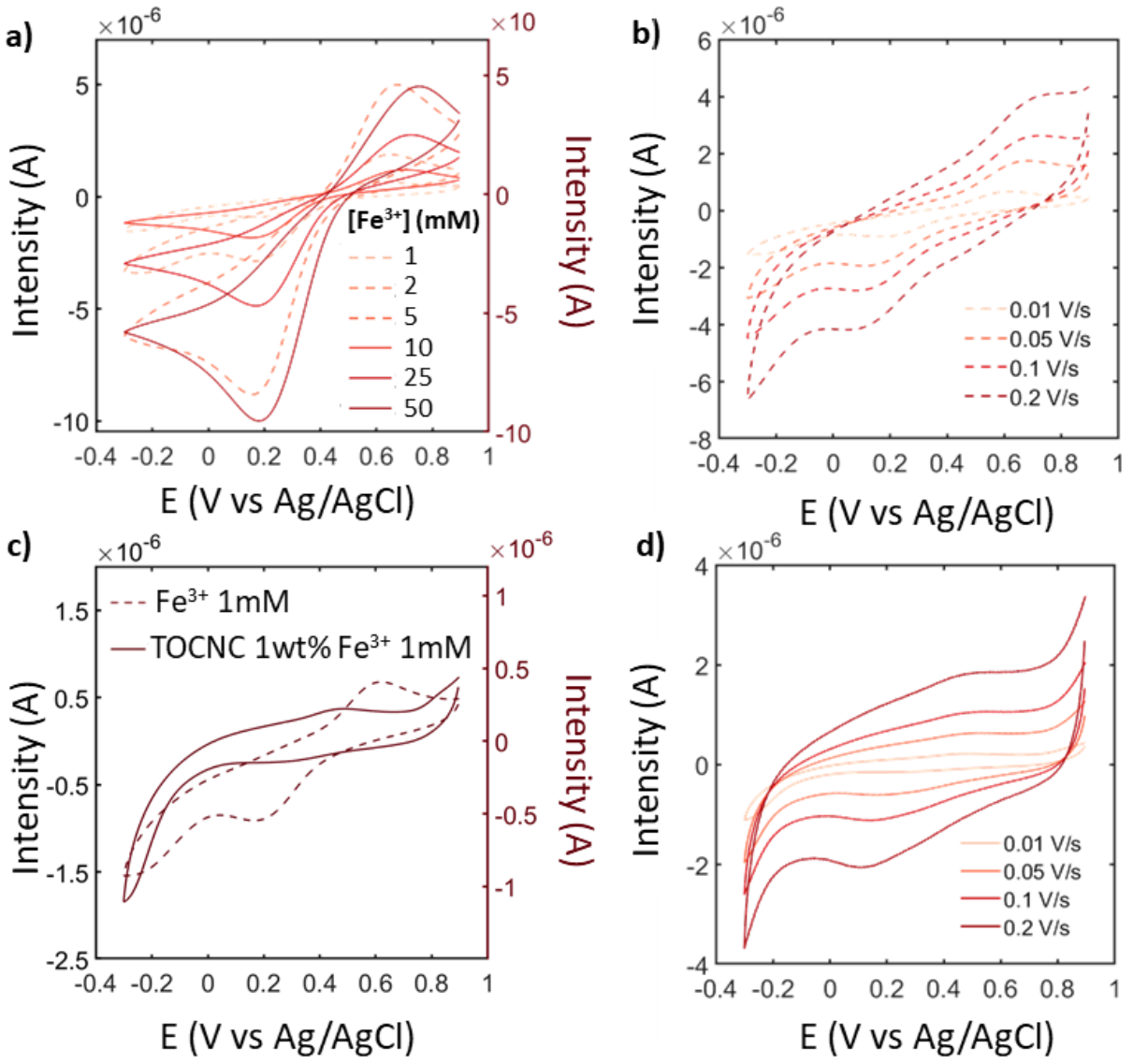


**Fig. S6.** a) Cyclic voltammograms obtained for different concentrations of $Fe^{3+}$ ions acquired with a scan rate of 0.01 V/s. The dashed and the solid lines refer to the left and right y-axis, respectively. b) Cyclic voltammograms obtained for $Fe^{3+}$ 1 mM at different scan rates. c) Cyclic voltammograms of a solution of $Fe^{3+}$ 1 mM in the absence (dashed line, left y-axis) and in the presence (solid line, right y-axis) of TOCNC, highlighting the shift of the anodic and cathodic peaks potentials in the presence of TOCNC. d) Cyclic voltammograms obtained for $Fe^{3+}$ 1 mM in the presence of TOCNC 1wt% at different scan rates.

## 3. Pore size distribution of the TOCNC networks at different $Fe^{3+}$ concentrations

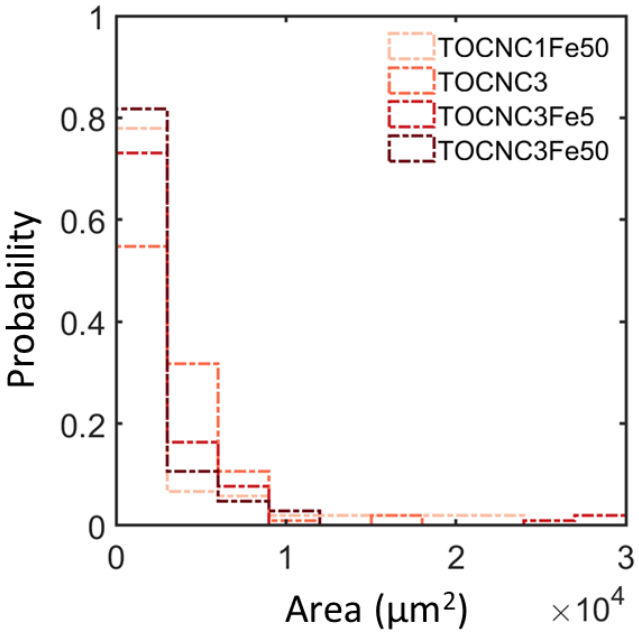


**Fig. S7.** Probability Distribution of the pores area of TOCNC 1 wt% and 3 wt% in the presence of different $Fe^{3+}$ ions concentrations. The area of the pores has been measured by Photoshop ImageJ software®[2] from the SEM images reported in Fig. 4d (i) TOCNC1Fe50, (ii) TOCNC3Fe0, (iii) TOCNC3Fe5 and (iv) TOCNC3Fe50 in the main text.

## 4. Modelling the $Fe^{3+}$-driven self-assembly of TOCNC

The pipeline for MD simulation is sketched in Scheme S1.

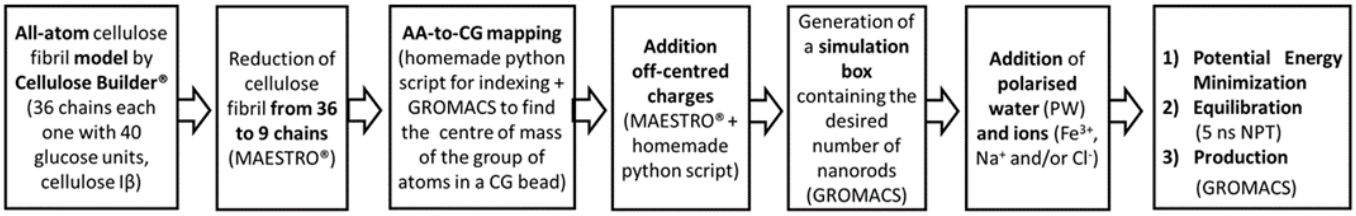


**Scheme S1.** Pipeline of the model preparation and production of the MD trajectories with specified software and scripts used at each step.

*Building the all-atom CNC model*

A starting pdb file containing all-atoms coordinates and H-bond information for cellulose Iβ fibril constituted of 36 chains of 40 glucose units each was generated using the on-line available software Cellulose Builder[3] and then modified by MAESTRO®, SCHROEDINGER[4](academic license) to reduce the number of chains to 9. Importantly, the chosen model includes a bulk cellulose chain, which exclusively establish cellulose-cellulose interactions and do not interact with the surrounding solvent and ions. The number of repeating glucose units per chains was chosen to approximately maintain the aspect ratio of the experimental sample, as reported in Table S10.

**Table S4.** Aspect ratio of the cellulose nanorods in the experimental sample and in the All-Atoms and Coarse-Grained models.

| System | Width & Length | Aspect Ratio |
|---|---|---|
| *Experimental Sample* | 8-15 nm width<br>100-150 nm length | ~ 10 |
| *TOCNC_9X40 AA* | 2.34 nm width<br>21.1 nm length | ~ 9 |
| *TOCNC_9x40 CG* | 2.21 nm width<br>20.5 nm length | ~ 9 |

*CNC all-atom to coarse-grained mapping*

Starting from our all-atom (AA) model of CNC, we performed all-atom to coarse-grained (AA-to-CG) mapping following beads assignment reported by Lopez et al.,[5, 6] where approximately 4 heavy atoms are grouped into one bead, each glucohexopyranose ring is represented by 3 beads, and cellobiose is taken as minimum repeating unit (see Fig. 5a in the Main Text). *Note:* we have exchanged the labels B4 and B5 in Table 1 (angles and dihedrals) and Table 2 of the original paper.[6]

A homemade python script was created to generate the list of the atomistic atoms contained in each bead. Following, the *gromacs* tool *traj* was used to output the centres of mass of the grouped atoms. To each bead, a bead type was associated (Table S11). The different bead types reflect the degree of polarity of the atom groups (P denotes polar beads, with polarity increasing from P1 to P4, and PX is specific of cellulose I$\beta$). The bonded interactions parameters (harmonic bonds length, angular potentials and proper dihedrals) used corresponds to the ones reported by Lopez et al.,[6] while non-bonded interactions (12-6 Lennard-Jones and Coulombic potentials) are taken from the martini_v2.3P force field.[7]

*Conversion from CNC to TOCNC: introduction of negative charges*

In TOCNC nanorods, the TEMPO-oxidation exclusively acts on the surface C6 hydroxymethyl groups. Specifically, taking cellobiose as repeating unit, one glycosyl unit outwards exposes the hydroxymethyl group, while the other points towards the bulk cellulose chains. For the conversion of the hydroxymethyl into a carboxylic acid functional group in our model, we took inspiration from the changes from protonated to deprotonated glutamate in Martini 2P.[8] Hence, we defined a different cellulose model in which the surface B3 or the B6 beads of the cellobiose unit are replaced by the negatively charged bead type Qa, and called the associated bead BX. Embedded charges were then introduced by an off-centre charge model with a negative unit charge located on a virtual site of mass 0, connected to the centre of the bead by a bond of length 0.11 nm and described by a 2fd geometry.[8] Hence, we decorated our model, comprised of 360 glycosyl units, with a total number of 100-unit charges (equal to the electron charge), allocated as shown in the main text, Fig. 5b. This number is slightly smaller than the value estimated based on the reported carboxylic content in the experimental sample (2 mmol/g, *i.e.*, 1/3 of the glucosyl units), but it is expedient to obtain a regular distribution of charges on the rods' surface.

**Table S5.** Mapping of atoms to CG beads, beads name and bead types for the developed models.[6] Numbering of the glucohexopyranose ring is reported in the main text, Fig. 1.

| AA-to-CG mapping | | Bead name | Bead type | |
|---|---|---|---|---|
| Cellobiose units | | | CNC | TOCNC |
| | C2, O2, C3, O3 | B1 | P4 | |
| | C1, C4, O4, O5 | B2 | PX | |
| | C5, C6, O6 | B3/BX | P1 | P1/Qa |
| | C1, C4, O4, O5 | B4 | PX | |
| | C2, O2, C3, O3 | B5 | P4 | |
| | C5, C6, O6 | B6/BX | P1 | P1/Qa |

*CG model of water and ions*

Herein, we used the MARTINI Polarizable Water (PW) v2.3P force field. Given the crucial role of water, its treatment is essential to derive information from simulation studies. Water modelled as van der Waals particles lacks the effect of polarisation and screening of interactions depending on the local environment. In the PW model, however, water is represented as a three-bead composed by four water molecules which accounts for the orientational polarizability of real water.[8, 9] Parameters for the $Na^+$ and $Cl^-$ ions were taken from martini_v2.0_ions.itp file, subsequently modified for the introduction of $Fe^{3+}$ ions.

*Simulation setup*

In the intention to mimic the experimental conditions investigated, we constructed three systems with TOCNC 1wt% and TOCNC 3wt% in the presence of $Fe^{3+}$ ions 5 and 50 mM, as summarised in Table S12. Table S13 reports the simulation parameters for the TOCNC 1wt% sample, which contains 2 rods; for the TOCNC 3 wt% model, a box with the same size was kept and 6 rods inserted.

**Table S6.** Schematic description of the systems constructed to model TOCNC 1wt% and 3wt% with 5 and 50 mM of $Fe^{3+}$ ions.

| Simulated system | Number of rods | $Fe^{3+}$ concentration | Number of $Fe^{3+}$ atoms | Number of $Na^{+}$ atoms |
|---|---|---|---|---|
| *TOCNC1Fe50* | 2 | 50 mM | 600 | - |
| *TOCNC3Fe5* | 6 | 5 mM | 60 | 420 |
| *TOCNC3Fe50* | 6 | 50 mM | 600 | - |

**Table S7.** Simulation setup for the TOCNC 1wt% system.

| | |
|---|---|
| Cubic Box, side length L= 27 nm | $V = L^3 = 19683\ nm^3 = 1.9683\ E^{-17}\ cm^3 = 1.9683\ E^{-17}$ ml |
| TOCNC_9X40 | 1 mol = 58482 g |
| for TOCNC 1wt%, 10 mg are dispersed in 1 mL solution, hence: | |
| TOCNC_9X40 | $1.71 \times 10^{-7}$ mol in 1 mL |
| | $3.366 \cdot 10^{-24}$ mol in $1.9683\ 10^{-17}$ ml |
| $3.366 \cdot 10^{-24}$ mol of TOCNC_9X40 correspond to number of rods ($N_{rods}$): | |
| $N_{rods} = N_{moles} \times N_A = 3.366\ 10^{-24} \times 6.0221\ 10^{24} = 2.03 \cong 2$ | |

In the TOCNC1Fe50 system the two rods were initially placed in a parallel orientation at a 100 Å distance. In the TOCNC3Fe5 and TOCNC3Fe50 systems, instead, an initial random configuration was obtained with the *gromacs* tool *insert-molecules*. The rods were placed in a cubic box with side dimension L=27 nm, under periodic boundary conditions, and then solvated by 130000 polarizable MARTINI water beads. The latter were then replaced with the required number of $Fe^{3+}$ ions to obtain the desired concentrations. When needed, additional $Na^{+}$ or $Cl^{-}$ ions were added to balance charges. Energy minimization was performed using the steep descent algorithm. Then, 5 ns isothermal-isobaric (NPT) simulation was run with a timestep of 20 fs and leap-frog algorithm.[10] Constant temperature (300 K) was achieved by separately coupling the TOCNC rods and the water and ions to a Berendsen thermostat,[11] while constant pressure (1 bar) was obtained by coupling to a Berendsen barostat.[11] Coulombic interactions were treated with particle-mesh Ewald method with $\varepsilon = 2.5$, while short-range electrostatics and van der Waals interactions were cut off at a 1.2 nm distance.

Finally, production trajectories were calculated in the NPT ensemble using the leap-frog integrator, v-rescale temperature coupling[12] and Parrinello-Rahman pressure coupling[13] schemes, with a reference temperature of 300 K and pressure of 1 atm. LINCS[14] was used to constrain the MARTINI polarizable water dummy bonds. Production trajectories were run for 100 ns (TOCNC3Fe5) and 150 ns (TOCNC1Fe50 and TOCNC3Fe50). For all trajectories the equations of motion were integrated using leap-frog algorithm,[10] with a timestep of 20 fs.

*Analysis of the trajectories*

To characterise our systems, we calculated the relative positions and angles between TOCNC rods, the radial distribution function (RDF) between TOCNC nanorods and between TOCNC and $Fe^{3+}$ ions, and the survival probability of $Na^{+}$, $Fe^{3+}$ or water in the proximity of the rods.

The GROMACS toolkit *angle* was used to compute the dihedral angle between nanorods[15, 16] and consequently their relative position. The RDF toolkits available on VMD[17] was used to compute contacts between cellulose nanorods and between the cellulose nanorods and $Fe^{3+}$ ions.

The survival probability, $P(\tau)$, which defines the average fraction of particles within the distance d from a certain site at a certain time $t$, that remains there at a time $t' = t + \tau$, was calculated following the procedure described by Araya-Secchi et al.[18] For the results shown in the plots in Figure 5c(ii), d = 7 Å was assumed; the survival probabilities and the corresponding error bars were calculated as arithmetic means and standard deviations, respectively, over 5 segments, each of 10 ns, of the final 50 ns of the MD trajectory. For the calculation of survival probabilities and contact distances the algorithm available in the open-source software MDAnalysis[19] were used.

*Calculation of the total surface charge on TOCNC nanorods*

**Table S8.** Charges of adsorbed cations and total charge on the surface of TOCNC rods, from MD simulations of TOCNC1Fe50, TOCNC3Fe5 and TOCNC3Fe50 in water. The total surface charge on a TOCNC rod is calculated as the sum of its negative charges (-100) and the charges of adsorbed cations. The electron charge (in absolute value) is taken as the unit.

| System | | ROD1 | ROD2 | ROD3 | ROD4 | ROD5 | ROD6 |
|---|---|---|---|---|---|---|---|
| **TOCNC1Fe50** | **$Fe^{3+}$ charges** | +90 | +75 | - | - | - | - |
| | **Total surface charge** | -10 | -25 | | | | |
| **TOCNC3Fe5** | **$Fe^{3+}$ charges** | +12 | +27 | +12 | +24 | +12 | +18 |
| | **$Na^{+}$ charges** | +36 | +30 | +34 | +21 | +21 | +48 |
| | **Total surface charge** | -52 | -43 | -54 | -55 | -67 | -34 |
| **TOCNC3Fe50** | **$Fe^{3+}$ charges** | +93 | +57 | +78 | +102 | +90 | +93 |
| | **Total surface charge** | -7 | -43 | -22 | +2 | -10 | -7 |

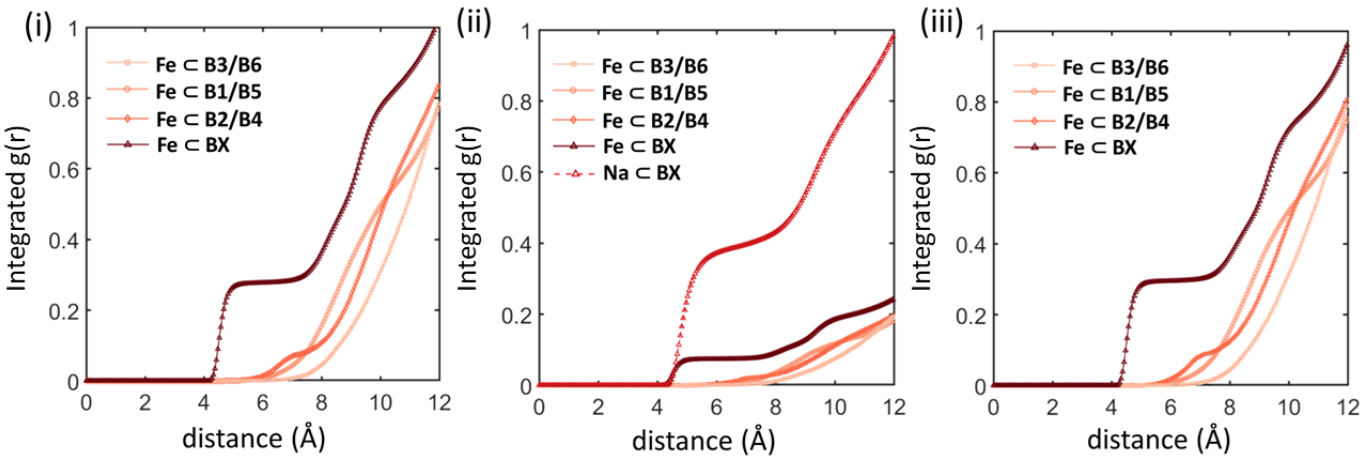


**Fig. S8.** Integral of the radial distribution function between the cellulose beads and the $Fe^{3+}$ ions for (i) TOCNC1Fe50, (ii) TOCNC3Fe5 and (iii) TOCNC3Fe50 systems.

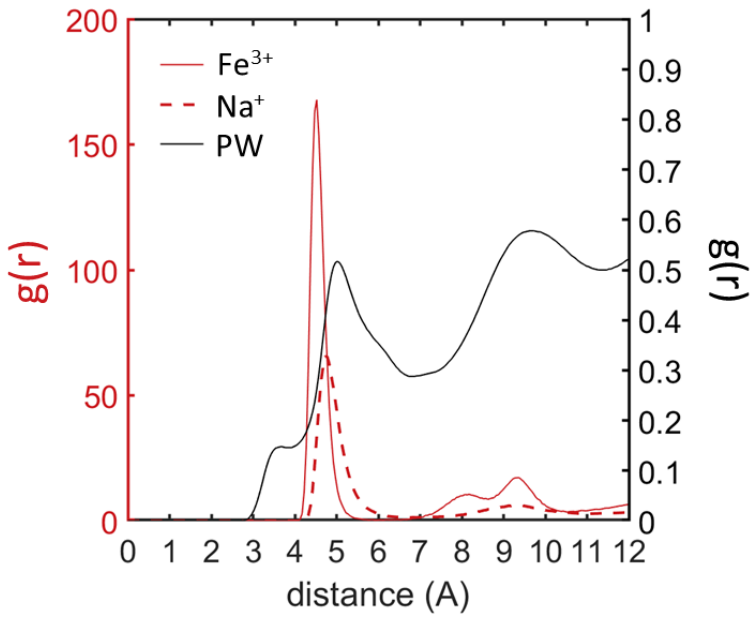


**Fig. S9.** Left y-axis: RDF of $Fe^{3+}$ (solid red line) and $Na^{+}$ (dashed red line) around BX in the TOCNC3Fe5 system; right y-axis: RDF of PW around the cellulose nanorods in the TOCNC3Fe5 system.

*Point of contacts and relative orientation between nanorods*

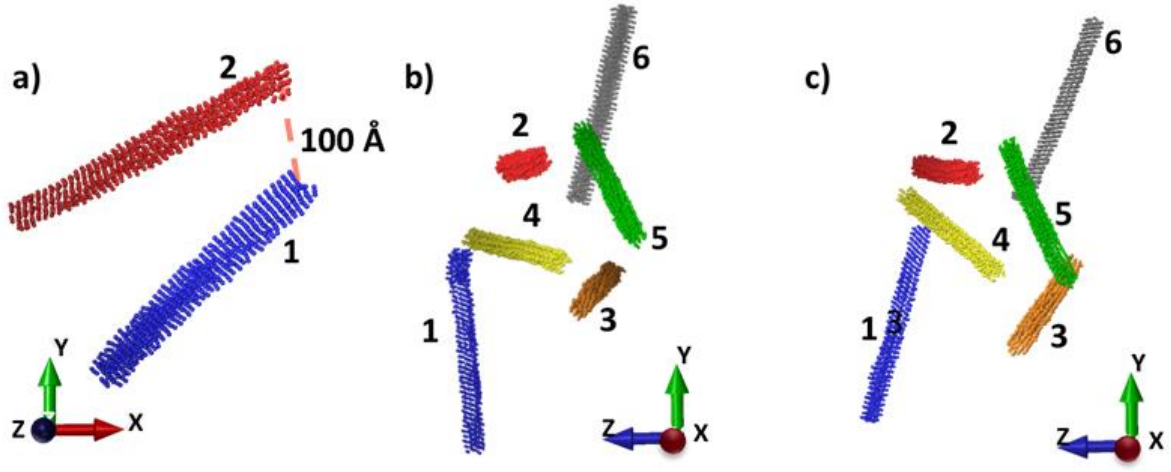


**Fig. S10.** Snapshot of a) TOCNC1Fe50, b) TOCNC3Fe5 and c) TOCNC3Fe50 at the beginning of the MD trajectory. To facilitate the visualization, the assigned rod numbers are reported.

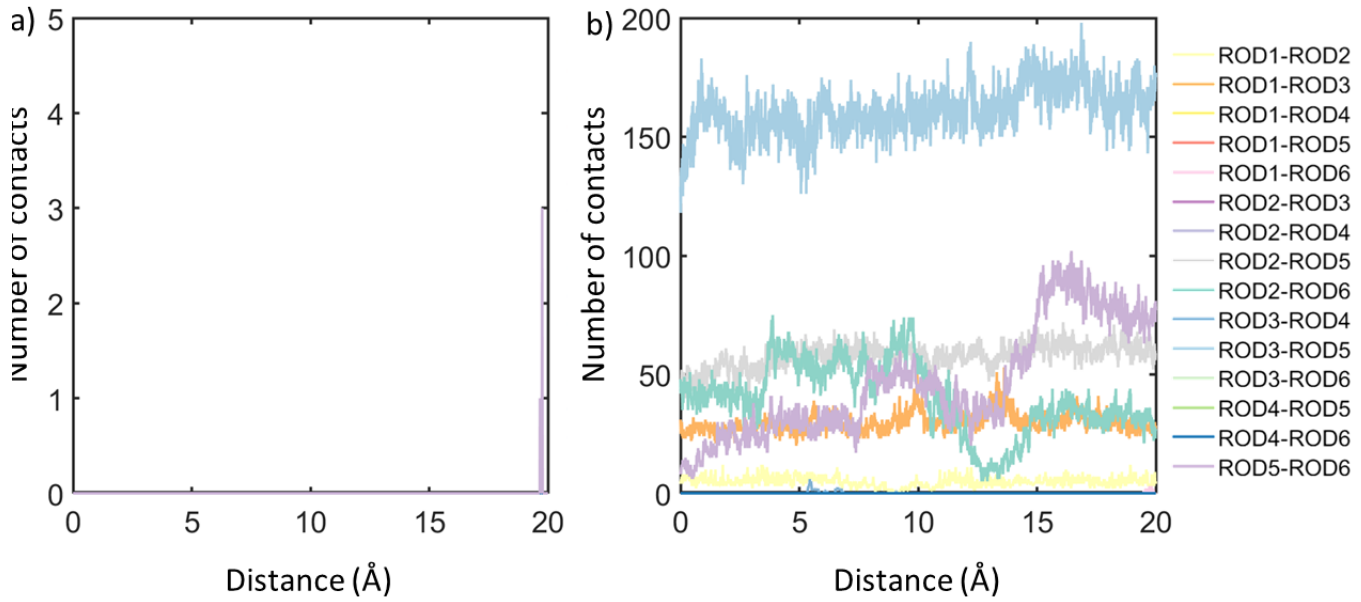


**Fig. S11.** Number of contacts between TOCNC rods along the final 50 ns of the trajectory of (a) TOCNC3Fe5 and (b) TOCNC3Fe50. A contact is defined by a distance equal or less than 20 A between a pair of beads.

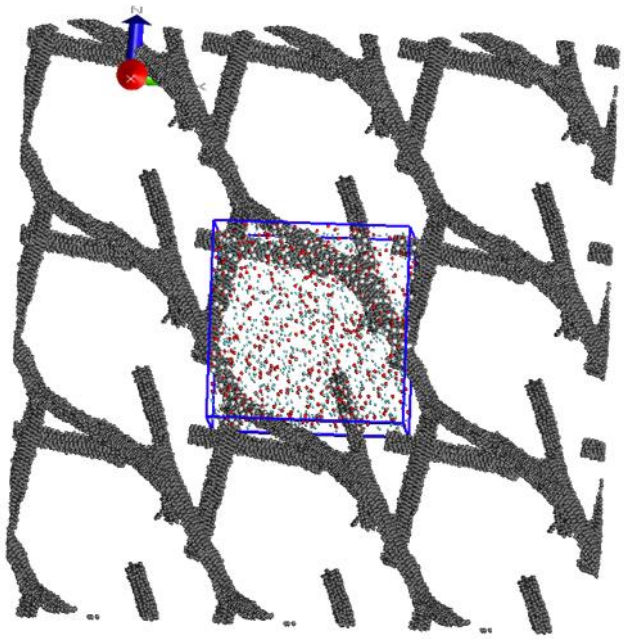

**Fig. S12.** Snapshot of the TOCNC3Fe50 system, with the central box surrounded by its periodic images (where only rods are shown).

## REFERENCES


(1) Fullerton, G. D.; Potter, J. L.; Dornbluth, N. NMR relaxation of protons in tissues and other macromolecular water solutions. *Magnetic resonance imaging.* **1982**, *1* (4), 209-226.

(2) Schneider, C. A.; Rasband, W. S.; Eliceiri, K. W. NIH Image to ImageJ: 25 years of image analysis. *Nature Methods* **2012**, *9* (7), 671-675.

(3) Gomes, T. C. F.; Skaf, M. S. Cellulose-Builder: A toolkit for building crystalline structures of cellulose. *Journal of Computational Chemistry* **2012**, *33* (14), 1338-1346.

(4) *Schrödinger Release : 2021-1, Maestro, Schrödinger*; New York, NY, 2021.

(5) López, C. A.; Rzepiela, A. J.; De Vries, A. H.; Dijkhuizen, L.; Hünenberger, P. H.; Marrink, S. J. Martini Coarse-Grained Force Field: Extension to Carbohydrates. *Journal of Chemical Theory and Computation* **2009**, *5* (12), 3195-3210.

(6) López, C. A.; Bellesia, G.; Redondo, A.; Langan, P.; Chundawat, S. P. S.; Dale, B. E.; Marrink, S. J.; Gnanakaran, S. MARTINI Coarse-Grained Model for Crystalline Cellulose Microfibers. *The Journal of Physical Chemistry B* **2015**, *119* (2), 465-473.

(7) Khan, H. M.; Souza, P. C. T.; Thallmair, S.; Barnoud, J.; De Vries, A. H.; Marrink, S. J.; Reuter, N. Capturing Choline–Aromatics Cation−π Interactions in the MARTINI Force Field. *Journal of Chemical Theory and Computation* **2020**, *16* (4), 2550-2560.

(8) Yesylevskyy, S. O.; Schäfer, L. V.; Sengupta, D.; Marrink, S. J. Polarizable Water Model for the Coarse-Grained MARTINI Force Field. *PLoS Computational Biology* **2010**, *6* (6), e1000810.

(9) De Jong, D. H.; Singh, G.; Bennett, W. F. D.; Arnarez, C.; Wassenaar, T. A.; Schäfer, L. V.; Periole, X.; Tieleman, D. P.; Marrink, S. J. Improved Parameters for the Martini Coarse-Grained Protein Force Field. *Journal of Chemical Theory and Computation* **2013**, *9* (1), 687-697.

(10) Hockney, R. W., Goel, S. P., and Eastwood, J. W. Quiet high-resolution computer models of a plasma. . *Journal of Computational Physics* **1974**, *14(2)*, 148–158.

(11) Berendsen, H. J. C.; Postma, J. P. M.; Van Gunsteren, W. F.; Dinola, A.; Haak, J. R. Molecular dynamics with coupling to an external bath. *The Journal of Chemical Physics* **1984**, *81* (8), 3684-3690.

(12) Bussi, G.; Donadio, D.; Parrinello, M. Canonical sampling through velocity rescaling. *The Journal of Chemical Physics* **2007**, *126* (1), 014101.

(13) Parrinello, M.; Rahman, A. Polymorphic transitions in single crystals: A new molecular dynamics method. *Journal of Applied Physics* **1981**, *52* (12), 7182-7190.

(14) Hess, B.; Bekker, H.; Berendsen, H. J. C.; Fraaije, J. G. E. M. LINCS: A linear constraint solver for molecular simulations. *Journal of Computational Chemistry* **1997**, *18* (12), 1463-1472.

(15) H. Bekker, H. J. C. B., E.J. Dijkstra, S. Achterop, R. van Drunen, D. van der Spoel, A. Sijbers, H. Keegstra and M.K.R. Renardus. Gromacs: A parallel computer for molecular dynamics simulations. *Physics computing* **1993**, *92*, 252–256.

(16) Van Der Spoel, D.; Lindahl, E.; Hess, B.; Groenhof, G.; Mark, A. E.; Berendsen, H. J. C. GROMACS: Fast, flexible, and free. *Journal of Computational Chemistry* **2005**, *26* (16), 1701-1718.

(17) Humphrey, W.; Dalke, A.; Schulten, K. VMD: Visual molecular dynamics. *J Mol Graph Model* **1996**, *14* (1), 33-38.

(18) Araya-Secchi, R.; Perez-Acle, T.; Kang, S. G.; Huynh, T.; Bernardin, A.; Escalona, Y.; Garate, J. A.; Martinez, A. D.; Garcia, I. E.; Saez, J. C.; et al. Characterization of a novel water pocket inside the human Cx26 hemichannel structure. *Biophys J* **2014**, *107* (3), 599-612.

(19) Michaud-Agrawal, N.; Denning, E. J.; Woolf, T. B.; Beckstein, O. MDAnalysis: A toolkit for the analysis of molecular dynamics simulations. *Journal of Computational Chemistry* **2011**, *32* (10), 2319-2327.